TX. S1

At a temperature of -195.15℃, the nitrogen adsorption apparatus BSD-PS1 was used to calculate the Brunauer-Emmett-Teller specific surface area (S_{BET}) of the sample through the BET and Langmuir formulas by determining the adsorption amount at various pressure points. The adsorption equilibrium pressure was lowered by pumping out N_2 to obtain the adsorption-desorption isotherm, and the pore size, pore volume and pore size distribution of the samples were obtained by calculation. Powder X-ray diffraction (XRD) analysis of crystal structure and composition was carried out in continuous mode using a Rigaku D/max 2500X diffractometer equipped with a monochromatic Co Kα radiation source (α = 1.79026 Å) with an 18 kW high power rotating-target X-ray emitter over a range of 2θ values from 0 to 145°. The morphology and size distribution of the surface particles of the sample catalysts were evaluated by scanning electron microscopy (SEM) using a JSM-7800F field emission scanning electron microscope (FESEM) setup at accelerating voltages ranging from 0.01 to 30 kV. The samples were pulverized into powder and dispersed in a small amount of ethanol, sonicated for 15 min, and then the suspension was deposited onto porous carbon grids, and the morphology and microstructure of the sample catalysts were analyzed using a JEM-2010 transmission electron microscope (TEM) under an accelerating voltage of 80~200 kV. The elements Ru, Ce, Ni, and O and their chemical valences in the samples were analyzed by X-ray photoelectron spectroscopy (XPS) using an AXIS ULTRA DLD system and Al Kα radiation. The binding energy scale was established by setting the C 1s peak at 284.5 eV, allowing for the determination of the relative concentrations of the elements within the analyzed region. Electron paramagnetic resonance (EPR) was used to test the free radical species in the reaction solution using a Bruker EMX plus Xband CW EPR spectrometer at 2.00 mW (9.83 GHz) microwave conditions.

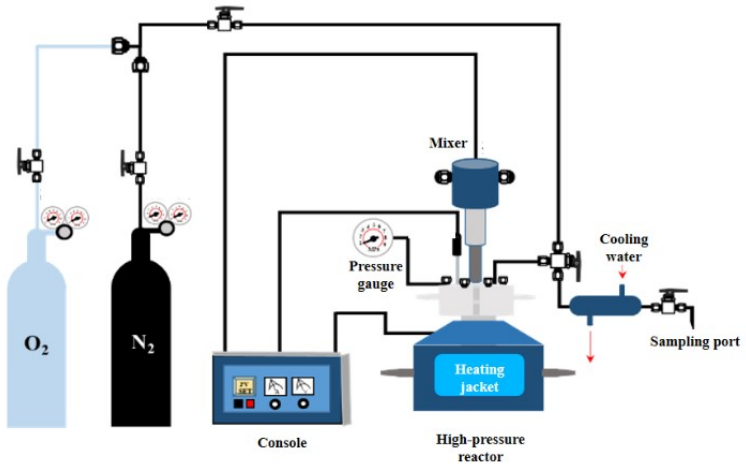

Fig. S1 Catalyst Evaluation System

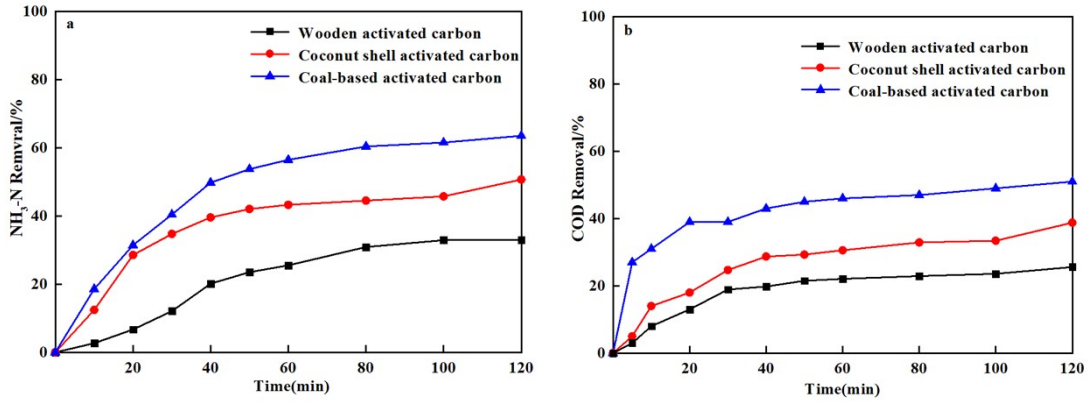

Fig. S2 (a) Effect of AC type on NH_3-N removal; (b) Effect of AC type on COD removal

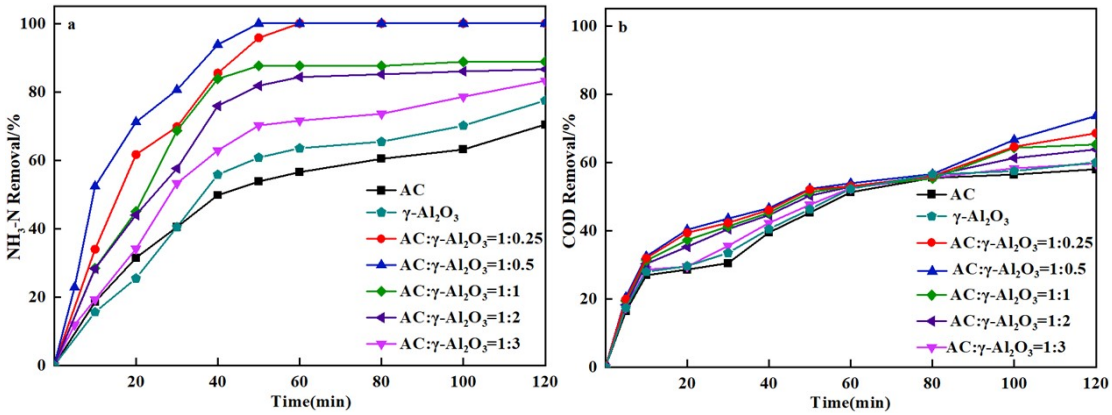

Fig. S3 (a) Effect of AAC ratio on NH_3-N removal; (b) Effect of AAC ratio on COD removal

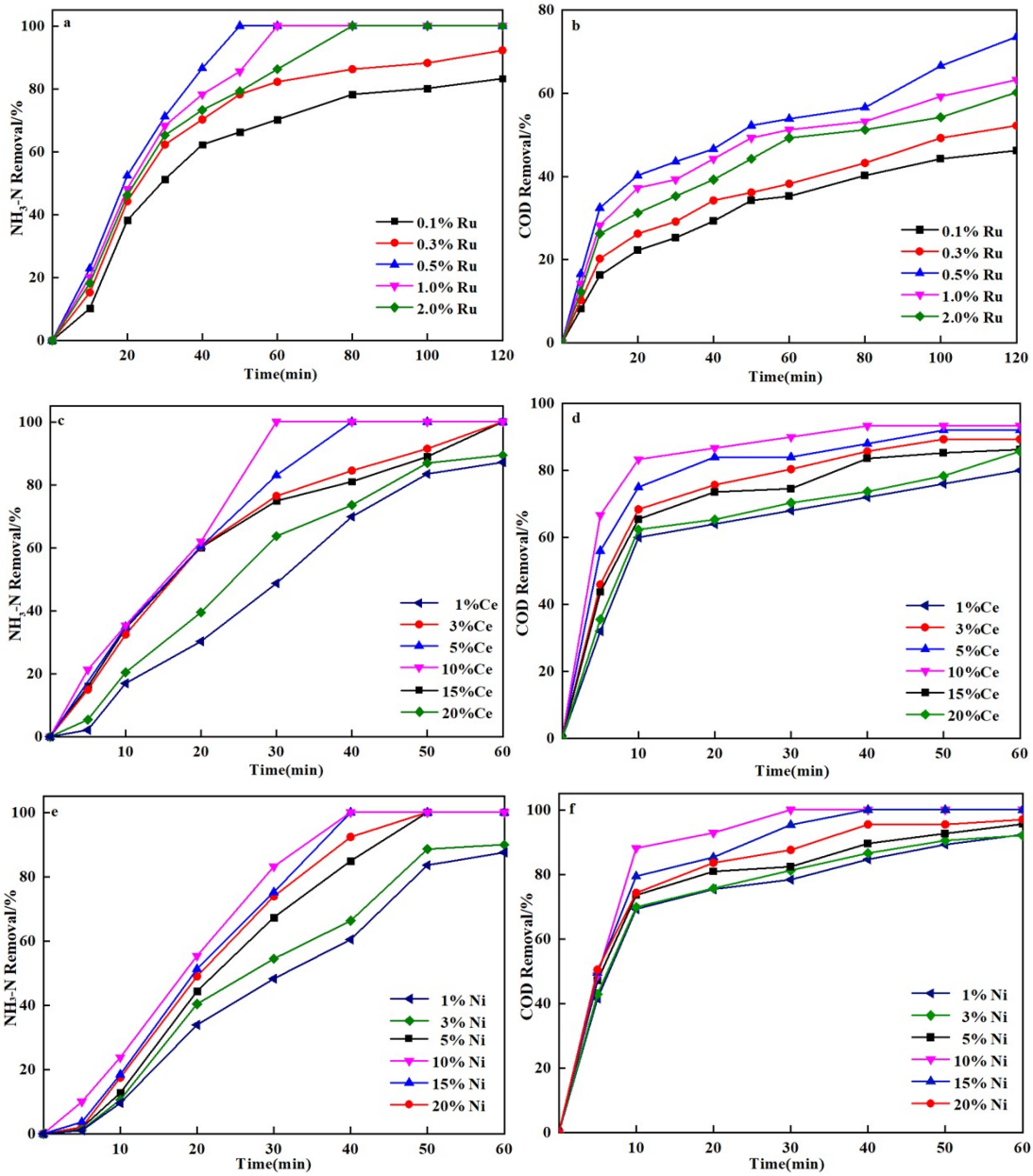

Fig. S4 (a) Effect of Ru loading on NH_3-N removal; (b) Effect of Ru loading on COD removal; (c) Effect of Ce loading on NH_3-N removal; (d) Effect of Ce loading on COD removal(e) Effect of Ni loading on NH_3-N removal; (f) Effect of Ni loading on COD removal

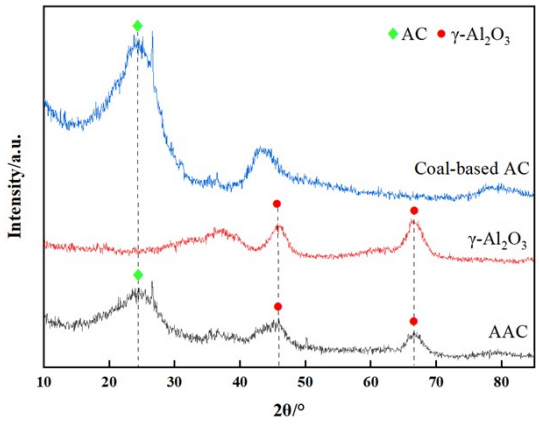

Fig. S5 XRD patterns of catalyst carrier components

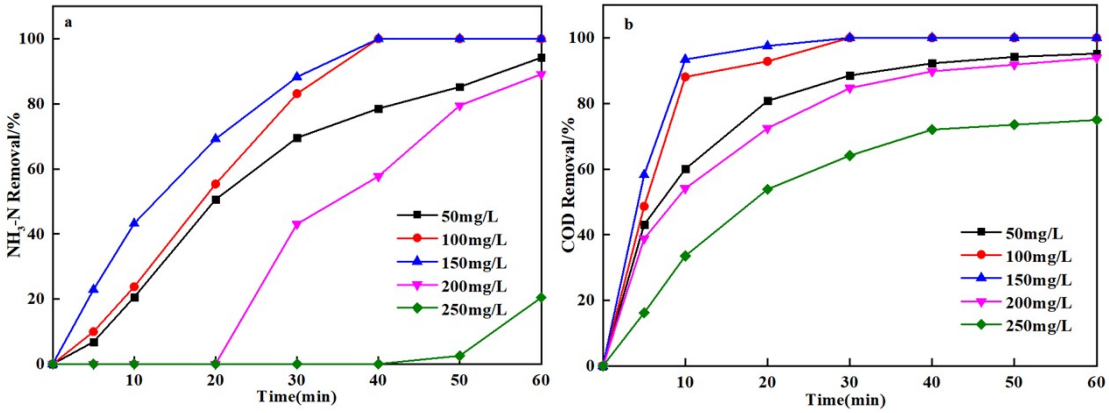

Fig. S6 (a) Effects of initial concentration on NH_3-N removal;(b) Effects of initial concentration on COD removal

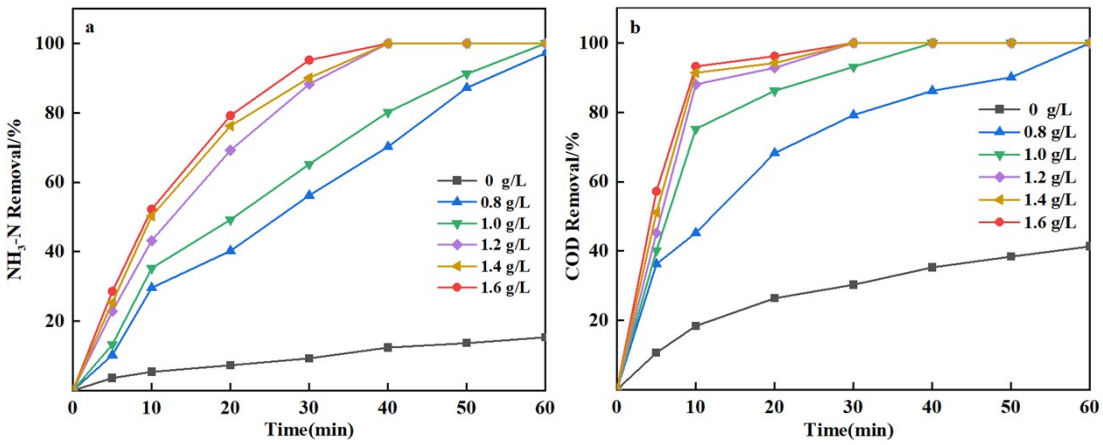

Fig. S7 (a) Effects of catalyst dosage on NH_3-N removal;(b) Effects of catalyst dosage on COD removal

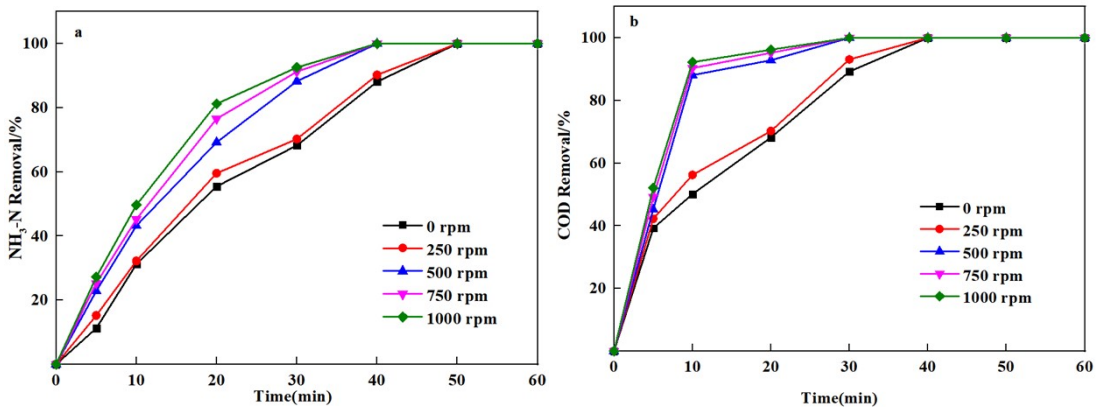

Fig. S8 (a) Effects of rotate speed on NH_3-N removal;(b) Effects of rotate speed on COD removal

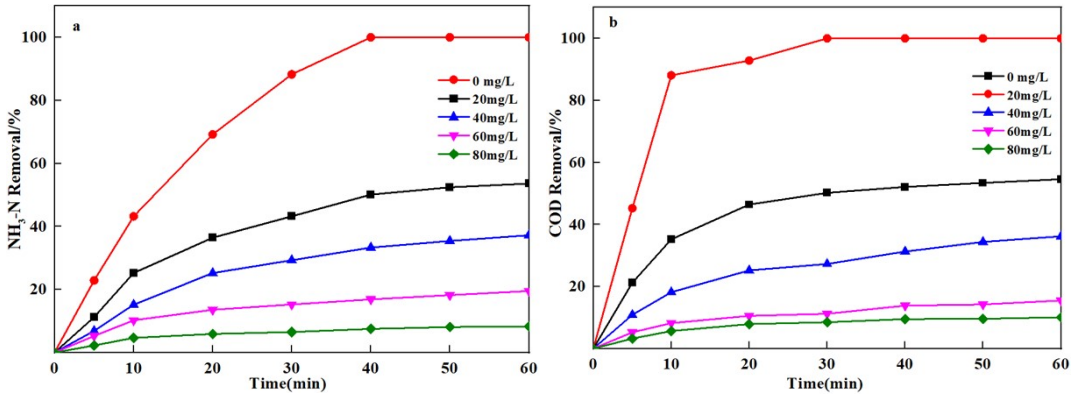

Fig. S9 (a)Effect of different concentrations of TBA on the removal of NH_3-N (b) Effect of different concentrations of TBA on the removal of COD

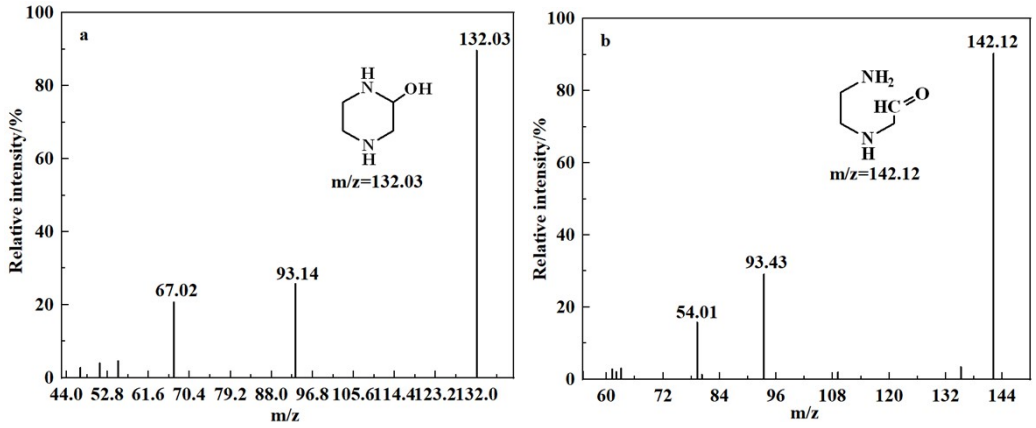

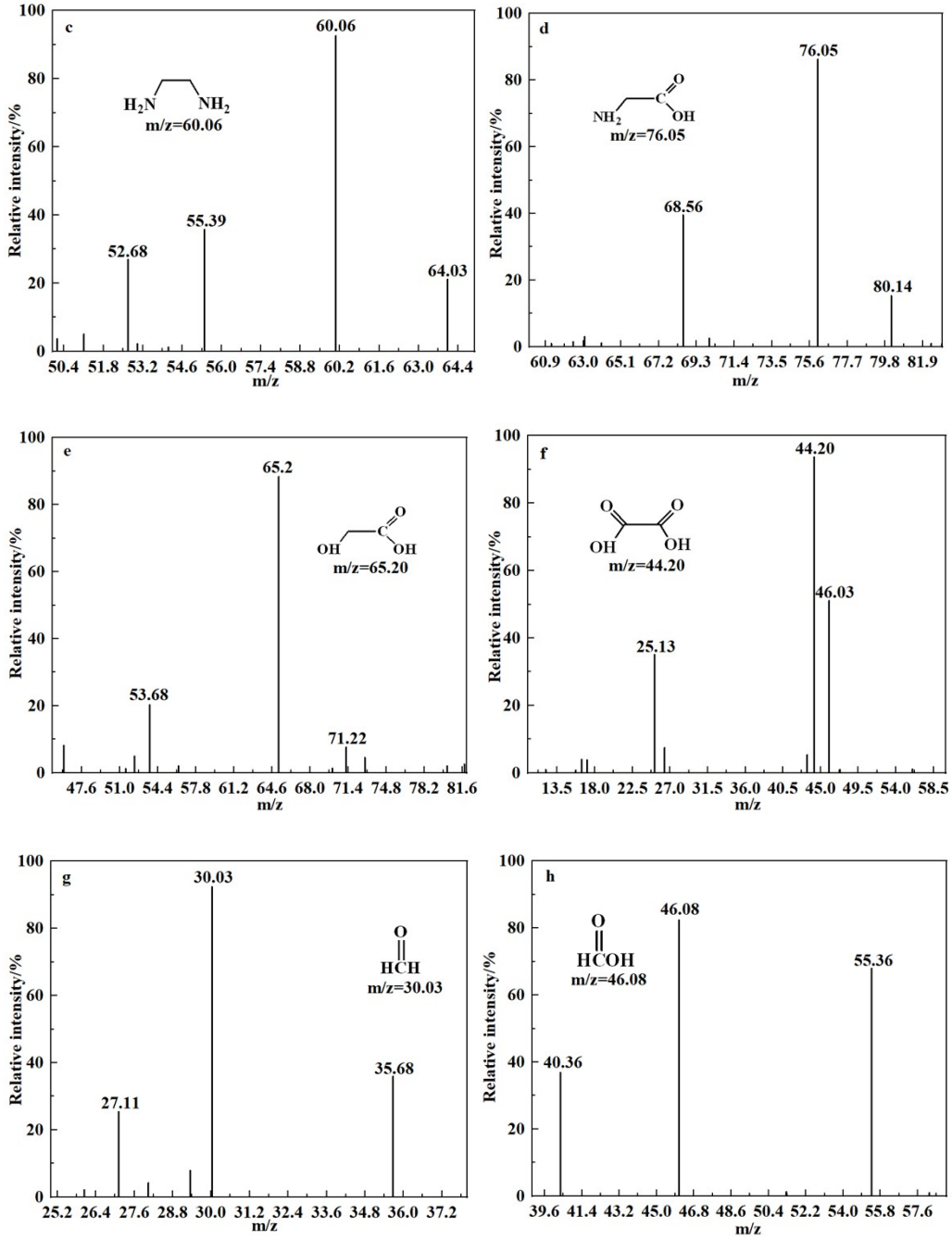

Fig. S10 Mass spectrum of the main intermediate product

(a) 2-Hydroxypiperazine, (b) [(2-aminoethyl) amino] acetaldehyde, (c) ethylenediamine, (d) glycine, (e) ethanoic acid, (f) oxalic acid, (g) formaldehyde, (h) formic acid